Atmospheric Science Letters

RMetS Royal Meteorological Society

RESEARCH ARTICLE OPEN ACCESS

The Two Arctic Wintertime Boundary Layer States: Disentangling the Role of Cloud and Wind Regimes in Reanalysis and Observations During MOSAiC

Sandro Dahlke[1] | Annette Rinke[1] | Matthew D. Shupe[2,3] | Christopher J. Cox[3]

[1]Alfred Wegener Institute, Helmholtz Centre for Polar and Marine Research, Potsdam, Germany | [2]Cooperative Institute for Research in Environmental Sciences, University of Colorado, Boulder, Colorado, USA | [3]NOAA Physical Sciences Laboratory (PSL), Boulder, Colorado, USA

Correspondence: Sandro Dahlke (sandro.dahlke@awi.de)

Received: 5 November 2024 | **Revised:** 1 April 2025 | **Accepted:** 2 April 2025

Funding: This work was by the Deutsche Forschungsgemeinschaft (DFG, German Research Foundation)—project no. 268020496–TRR 172, within the Transregional Collaborative Research Center "ArctiC Amplification: Climate Relevant Atmospheric and SurfaCe Processes, and Feedback Mechanisms (AC)3"; the European Union Horizon 2020 research and innovation programme: S.D. by grant agreement no. 101003826 (CRiceS) and A.R. by grant agreement no. 101003590 (PolarRES). C.C. and M.D.S. received support from NOAA's Global Ocean Monitoring and Observing Program through the Arctic Research Program (FundRef https://doi.org/10.13039/100018302) and the NOAA Physical Sciences Laboratory (NA22OAR4320151). M.D.S. was additionally supported by a Mercator Fellowship with (AC)3, the National Science Foundation (OPP-1724551), and Department of Energy (DE-SC0021341).

Keywords: atmospheric and climate dynamics | atmospheric physics | change and impacts | climate variability | field campaigns | radiation | synoptic | tools and methods

ABSTRACT

The wintertime central Arctic atmosphere comprises a radiatively clear and a radiatively opaque state, which are linked to synoptic forcing and mixed-phase clouds. Weather and climate models often lack process representations surrounding these states, but prior work mostly treated the problem as an aggregate of synoptic conditions, resulting in partially overlapping biases. Here, we disaggregate the Arctic states and confront ERA5 reanalysis with observations from the MOSAiC campaign over the central Arctic sea ice during winter 2019/2020. Low-level winds and liquid water path (LWP) are combined to derive different synoptic classes. Results show that the clear state is primarily formed by weak/moderate winds and the absence of liquid-bearing clouds, while strong winds and enhanced LWP primarily form the radiatively opaque state. ERA5 struggles to reproduce these basic statistics, shows too weak sensitivity of thermal radiation to synoptic forcing, and overestimates thermal radiation for similar LWP amounts. The latter is caused by a warm bias, which has a pronounced inversion structure and is largest in clear and calm conditions. Under strong synoptic forcing, the warm bias is constant with height and discrepancies in mixed-phase cloud altitude appear. Separating synoptic conditions is regarded as useful for process-oriented evaluation of the Arctic troposphere in models.

1 | Introduction

Walsh and Chapman (1998) and Vihma and Pirazzini (2005) showed that winter surface air temperatures over the central Arctic sea ice depend on both cloud and wind speed conditions, with a 15 K difference between the warmest (cloudy sky, strong wind) and coldest (clear sky, light wind) conditions. They also showed that wind changes (strong vs. light) cause similar temperature variations to the difference between cloudy and clear sky. Responsible processes include the control of cloud conditions by the synoptic weather situation as well as radiative fluxes and their interactions with clouds and the surface. Subsequently, Stramler et al. (2011) defined two synoptically driven distinct Arctic winter states over sea ice: warm cloudy (radiatively opaque, including mixed-phase clouds) and cold radiatively clear states, characterized by radiative surface cooling

and surface energy balance close to zero, and elevated inversions versus strong surface radiative cooling, negative surface energy balance, and surface-based temperature inversions (SBIs), respectively.

To better simulate the Arctic climate, an adequate understanding of the key processes regarding clouds and atmospheric boundary layer (ABL) dynamics over sea ice, and their controlling factors, such as synoptic forcing, is crucial. Previous observational studies have reported on links between atmospheric synoptic transport, cloud phase, and surface energy fluxes in winter (Tjernström and Graversen 2009; Persson et al. 2017). Related to this, the bimodal distribution in surface variables (net longwave radiation, temperature, wind) associated with the two states has been demonstrated for different regions of the Arctic (Stramler et al. 2011; Graham et al. 2017; Solomon et al. 2023). Most analyses focused on the different inversion characteristics (Stramler et al. 2011; Pithan et al. 2014), while the impact of these two states on the atmospheric vertical structure has rarely been studied. The existing studies often lack consideration of synoptic forcing, reporting biases in the aggregate of conditions or continuously (Day et al. 2024), although Persson et al. (2017) highlighted the role of synoptic variability by showing the dependency of related processes on two extreme (wet, dry) cloud liquid conditions. Here, diagnosing the synoptic forcing using co-varying subsets of wind-cloud conditions allows for the evaluation of the role of synoptic activity in producing the noted bimodality in atmospheric variables. ERA5 is one of the most advanced reanalyses regarding data assimilation and temporal resolution, and it indicates improved performance in the Arctic compared to other reanalyses (e.g., for wind fields, Graham, Hudson, et al. 2019; Graham, Cohen, et al. 2019). However, poor representation of sea ice (Arduini et al. 2022) and mixed-phase clouds limits key process representations over sea ice in winter, namely longwave radiation, surface temperature, turbulent heat fluxes, and SBIs (Graham, Cohen, et al. 2019; Herrmannsdörfer et al. 2023; Svensson et al. 2023)—which are biased in all reanalyses.

This paper addresses the following questions:

1. What is the signature of different cloud-liquid and wind regimes in the two wintertime ABL states?
2. How well are radiative processes and characteristic thermodynamic structures for each regime represented in a state-of-the-art atmospheric reanalysis?

For this, we compare ERA5 with observations from the Multidisciplinary drifting Observatory for the Study of Arctic Climate (MOSAiC) icebreaker expedition over the Central Arctic sea ice (Shupe et al. 2022) during November 2019–March 2020.

2 | Data and Methods

2.1 | Observations (OBS)

We utilize MOSAiC measurements from Met City (see Shupe et al. (2022) for details) on the sea ice adjacent to RV Polarstern for hourly means of longwave net (LWnet), downward (LWdown), and upward (LWup) radiative fluxes and 10 m wind speed (U10) (Cox et al. 2023). Hourly averages of liquid water content (LWC), liquid water path (LWP), ice water content (IWC), and ice water path (IWP) were retrieved using the Shupe–Turner approach (Shupe et al. 2015; Shupe 2022) combining multiple sensors operated onboard Polarstern. IWC and LWC have a vertical resolution of 50 m. Individual retrievals have an uncertainty of 49%–72% (5–25 gm^{-2}) for LWC and 62%–100% for IWC, respectively (Shupe et al. 2005, 2015). Corresponding (closest in time) temperature profiles are taken from Dahlke et al. (2023) where 6-hourly radiosondes and the 10-m tower are quality-controlled and blended to provide consistent profiles from the surface through the troposphere. Those have a vertical resolution of 5 m; below 10 m, however, observations are available at 0 m (skin temperature) and approximately 2 and 6 m.

2.2 | ERA5 Reanalysis

The same parameters as in the observations were extracted from hourly ERA5 atmospheric reanalysis (Hersbach et al. 2020) at 0.28125 degrees resolution, from which the grid point closest to MOSAiC was selected to match the observations each hour. For comparison, ERA5 profiles are linearly interpolated onto the same vertical axis as in the observations.

2.3 | Combined Synoptic Classes

We construct three "cloudiness" and three "windiness" classes based on rank-ordered observed U10 and LWP. This separation enables analysis of different combinations of wind and LWP classes—for example, contrasting liquid-bearing clouds under calm versus windy conditions. Information on the classes is summarized in Tables 1 and S1. While the U10 thresholds follow the inter-quartile range, the ones for LWP are somewhat arbitrary. This is because LWdown and LWP are related nonlinearly (Shupe and Intrieri 2004); for example, as little as 1 gm^{-2} LWP has a noticeable impact on LWdown (Figure S1), but more than 50% of OBS show 0 gm^{-2}. Conversely, mixed-phase clouds typically become radiatively opaque already around 30–35 gm^{-2} LWP (Shupe and Intrieri 2004; Persson et al. 2017). Based on these relations, and to ensure acceptable sample sizes for each class, the thresholds of 1 and 10 gm^{-2} were selected, respectively (Figure S2). We note that LWP uncertainty of individual retrievals exceeds those thresholds. However, we employ hourly averages, and furthermore, average over broad synoptic classes, which reduces the actual uncertainty and strengthens the robustness of class averages for selected parameters. To justify our approach, the clear impact of LWP on LWdown appears statistically detectable (Figure S1), even for bin sizes of 1 gm^{-2}. The LWP > 10 gm^{-2} condition agrees with the "wet" classification in Persson et al. (2017). Although low-level ice water in mixed-phase clouds also interacts with longwave radiation, we did not consider it in the construction of our classes, as its impact due to the lower optical depth is generally smaller than that of liquid water (Persson et al. 2017).

We also computed large-scale temperature advection to characterize synoptic forcing, but the results were difficult to connect to local observations; hence, this predictor was regarded as too

TABLE 1 | Parameter thresholds and overview for classifications.

Parameter	Threshold	Percentile	Meaning	Nomenclature
U10	$<3.1\,ms^{-1}$	<25th	Calm	W0
	$3.1–8.2\,ms^{-1}$	25th–75th	Windy	W1
	$>8.2\,ms^{-1}$	>75th	Very windy	W2
LWP	$<1\,gm^{-2}$	<66th	Clear	C0
	$1–10\,gm^{-2}$	66th–82nd	Cloudy	C1
	$>10\,gm^{-2}$	>82nd	Very cloudy	C2

unspecific for our disaggregation. We provide some discussion on this in the Supplement.

2.4 | Longwave Radiation and Synoptic Classes

Figure 1 shows how the combined LWP versus U10 classes contribute to longwave radiation components in OBS and ERA5. One can see the well-known bimodality in the observed LWnet distribution, with one peak around $-40\,Wm^{-2}$ representing the radiatively clear state and the radiatively opaque state with a second peak around $-5\,Wm^{-2}$ ($0\,Wm^{-2}$ in Stramler et al. 2011). ERA5 lacks this bimodality and has a positive LWup bias caused by a surface warm bias, as previously reported (Batrak and Müller 2019; Herrmannsdörfer et al. 2023). Here we extend upon this concept to show how those aspects of the longwave radiation components relate to certain combined synoptic classes. As expected, C1 and especially C2 classes strongly contribute to the radiatively opaque sector of the LWnet distribution—a clear indication of the radiative impact of liquid-bearing clouds (Shupe and Intrieri 2004; Morrison et al. 2012). In keeping with Walsh and Chapman (1998), W2 classes altogether also tend to favor the radiatively opaque state–a phenomenon fundamentally captured by ERA5. In OBS, however, W2C0 contributes roughly the same to this LWnet peak as W2C1–W2C2 together, while ERA5 is mostly representative of W2C0. Notably, the sub-classes are qualitatively distributed as expected in ERA5 in terms of the transitioning preponderance from one extreme to the other, even if the distribution shape differs between ERA5 and OBS. This is in part consistent with an underrepresentation of LWP in ERA5, reflected as lower occurrence of C2 classes in the right-side of the distribution. A complicating factor is that in both OBS and ERA5, the radiatively opaque state can also occur in the absence of liquid water, especially for W2 classes. Under such strong synoptic forcing, ice clouds (Miller et al. 2015), water vapor and advected warm air are often enhanced in the lower troposphere and impact LWdown as well. On the left side of the distribution, W1 and W0 classes essentially form the occurrence peak of the radiatively clear state—this is only partially represented in ERA5. ERA5 resembles the overall shape of the observed LWup distribution, but the reanalysis' prominent surface warm bias reflects in a median LWup overestimation by $11\,Wm^{-2}$ compared to OBS. Specifically, the frequently observed minimal LWup estimates of $170–180\,Wm^{-2}$ for the W0C0 class are uncommon in ERA5. Figure 2 provides a more comprehensive assessment of the average longwave radiation characteristics associated with each class. Consistent with Figure 1, LWup, LWdown and LWnet all show a proclivity to decrease as windiness and cloudiness decrease. ERA5 consistently underestimates LWdown for all C2 classes, which is due to underestimated LWP of about $20–25\,gm^{-2}$ and hence, lower emissivity. Figure S3 supports this finding, showing that average LWP for the C2 classes is lower in ERA5 than in OBS and averages around $15–25\,gm^{-2}$, a range where LWdown is sensitive to LWP (Figure S1), hence explaining the negative LWdown bias. Figure 2 also indicates that in ERA5, occurrence of these C2 classes is underrepresented by about 2%–5%. In contrast to C2 classes, ERA5 overestimates LWdown for all other classes. Figure 2 indicates that this is not due to a positive LWP bias of ERA5 that would enhance emissivity, but as evident from Figures 3 and 4, it is likely driven by a warm bias in the emitting layer enhancing LWdown. Figure 4 shows that ERA5 for C1 and C0 classes indeed has a warm bias in the lowermost 100 m, but partially even up to 3000 m. Their occurrence is also 2%–6% higher in ERA5 than in OBS (Figure 2), which further adds to ERA5's overall positive LWdown bias. Within the C0 classes, ERA5 overestimates the occurrence of W2C0 and W1C0, but underestimates the occurrence of W0C0, each by 2%–6%, indicating that U10 in clear conditions is slightly larger in ERA5 than observed. Apart from C0 classes, wind biases are mostly small and show no systematic pattern. This is a slight difference to the numerical weather prediction models evaluated in Solomon et al. (2023), who found positive U10 biases during cloudy conditions, while U10 was reasonably well represented during clear conditions.

The reanalysis' surface warm bias translates to LWup biases of $5–20\,Wm^{-2}$. This bias is present in all classes but is most strongly expressed for clearer and calmer conditions. For W0C0, the bias is largest ($20\,Wm^{-2}$). The aforementioned biases in LWdown and LWup are then re-enforcing cumulatively in LWnet. For the C2 classes, regardless of wind, both LWdown and LWup biases in ERA5 combine to produce a negative LWnet bias of about $10–15\,Wm^{-2}$, with average ERA5 LWnet of -15 to $-20\,Wm^{-2}$, where $-5\,Wm^{-2}$ is observed. These results help explain the lack of bimodality in the ERA5 LWnet distribution: the radiatively opaque state, which is strongly constrained by C2, is projected onto too large negative LWnet values. Those biases also persist in the C1 classes, although slightly weaker ($2–7\,Wm^{-2}$). This is despite LWdown being overestimated for C1 classes—i.e., the negative LWnet bias is then governed by the positive LWup bias in ERA5. Finally, C0 classes contain among the largest ERA5 biases for both LWup and LWdown. However, those biases, both being strongly positive, partially compensate each other in LWnet. This is

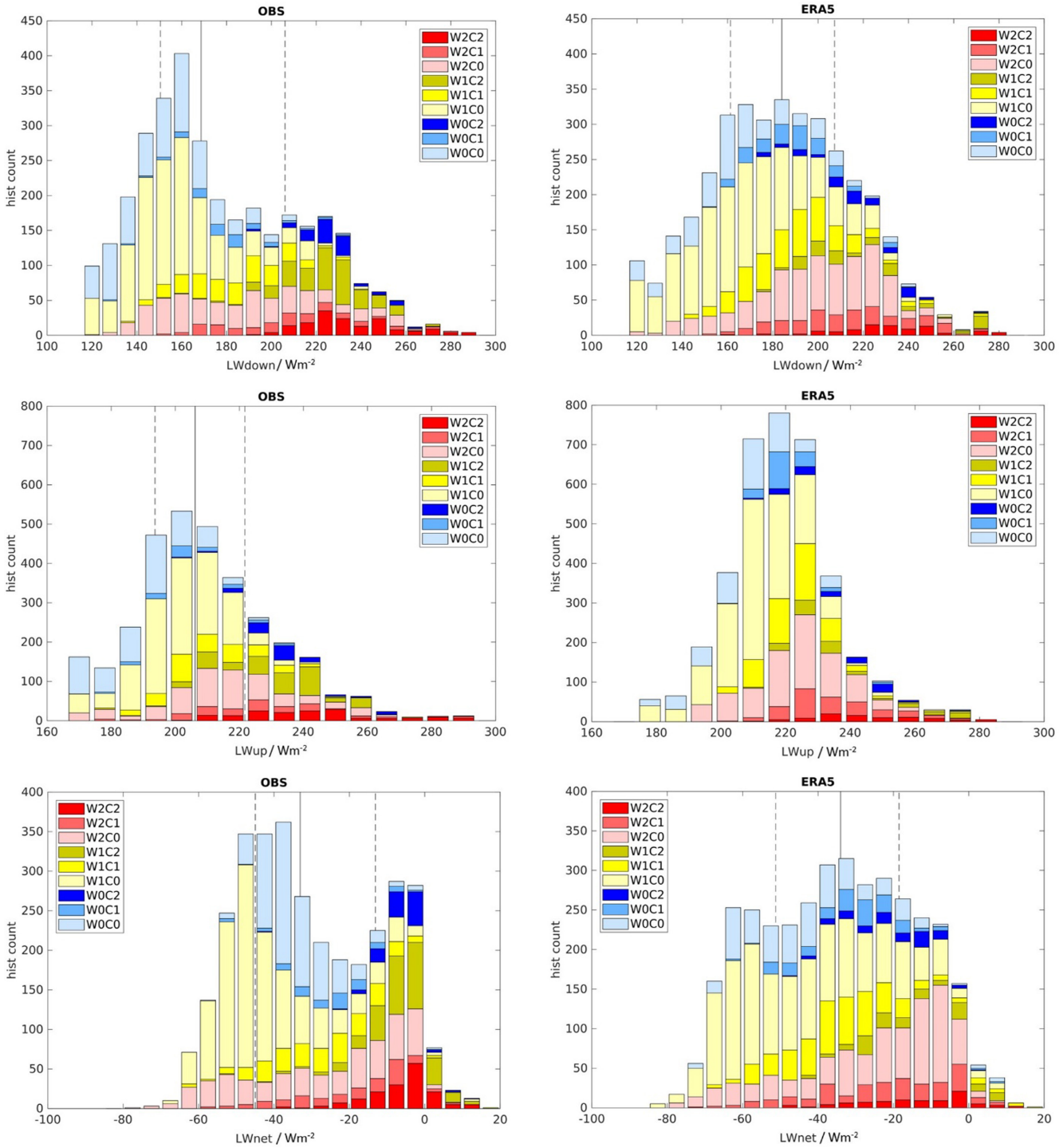

FIGURE 1 | Stacked histograms for hourly data of extended MOSAiC winter (NDJFM) LWdown (top), LWup (middle) and LWnet radiation (bottom) for OBS (left) and ERA5 (right). Different colors represent different U10 classes (reds = W2, yellows = W1, blues = W0), and different color intensities indicate LWP classes (light color = C0, normal color = C1, bold color = C2). Solid and dashed vertical lines represent the median and 25th/75th percentiles, respectively. Bin size is 5 Wm^{-2} for LWnet and 8 Wm^{-2} for LWdown and LWup.

consistent with the findings of Solomon et al. (2023). Apart from those features that are mostly independent of U10, there are also several aspects that depend on U10. This is evident, for example, in the sign and amplitude of ERA5's LWnet bias for the C0 classes. While the mean bias is +2.8 Wm^{-2} for W2C0, it is already weakly negative for W1C0 and ultimately strongly negative (−8.6 Wm^{-2}) during W0C0. This stems from the severity of the positive LWup bias, which is stronger under calmer conditions. This might be expected given ERA5's deficiencies in simulating conductive heat fluxes and lacking snow in the reanalysis (Batrak and Müller 2019), and poor representation of process-relationships between near surface stability and turbulent heat fluxes (Persson et al. 2017; Solomon et al. 2023).

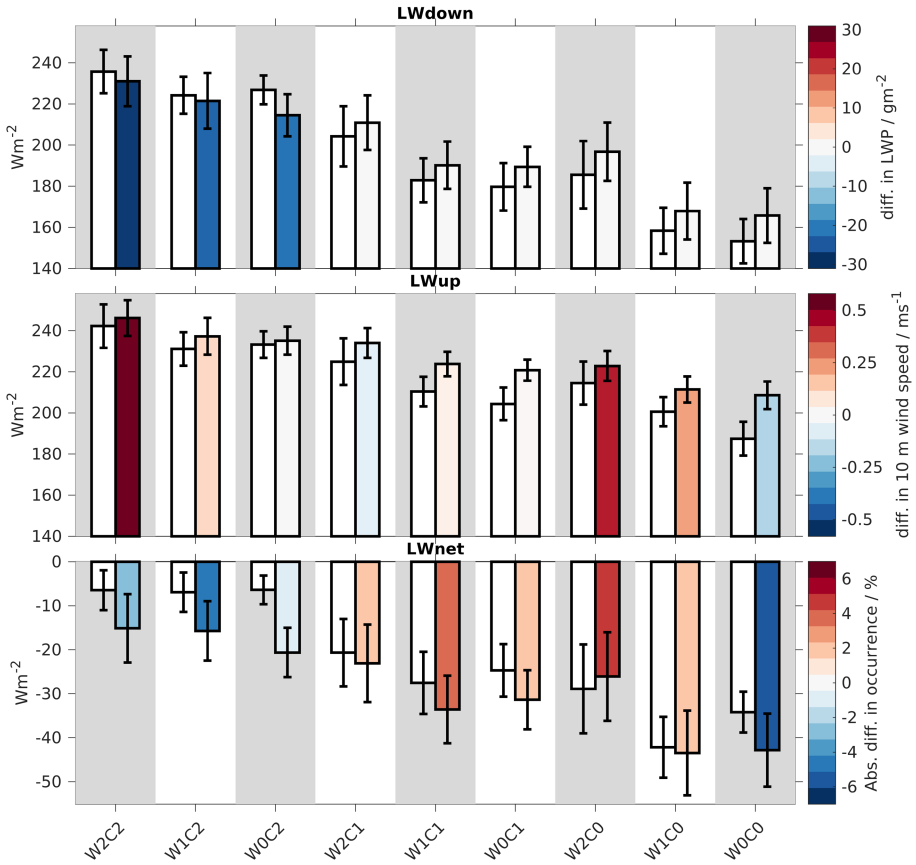

FIGURE 2 | MOSAiC winter (NDJFM) average LWdown (top), LWup (middle), and LWnet (bottom) for each of the combined synoptic classes. The white bar on the left for each class is for OBS, and the right bar for each class is ERA5, while the whiskers indicate ±1 standard deviation, respectively. The color of the ERA5 bar for each class indicates the absolute ERA5 minus OBS difference in LWP (top), U10 (middle), and occurrence frequency (bottom) of that class.

Using a somewhat different methodology, Persson et al. (2017) concluded that LWdown is enhanced by 60–100 Wm^{-2} during cloudy compared to clear periods. Our results agree with this range, but we additionally find for MOSAiC that the observed LWdown difference between the C2 and the C0 classes increases from 50 to 65 to 74 Wm^{-2} between the W2, W1, and W0 sub-classes, respectively (Figure 2). Hence, during calm conditions, the LWdown sensitivity to increases in LWP is larger than during windy conditions, which may point towards the potential to erode an inversion (clear) versus an already eroded inversion (cloudy). Those same numbers for ERA5 are 34, 54, and 49 Wm^{-2}, respectively. This shows that (a) ERA5 generally has a smaller sensitivity of LWdown to LWP changes and (b) the dependence of that sensitivity on U10, hence on the synoptic forcing, is less clear than in the observations.

2.5 | Thermodynamic Structure

Figure 3 presents average temperature, LWC, and IWC profiles for each class. Consistent with previous notions, the higher the LWP, the warmer the profiles, regardless of U10. In the lowermost 100 m in OBS, however, this temperature increase is larger for calmer conditions. For example, the temperature increase from C0 to C1 to C2 per class is 2–3 K under W2 conditions, which is enhanced to 5–6 K per class under W0 conditions. This is because enhanced mixing during stronger winds causes isothermal temperature profiles—SBIs exist primarily in the absence of liquid-containing clouds and during calm conditions, when shallow, stable ABLs are established through surface radiative cooling. This is, however, not seen in ERA5, which struggles to produce SBIs and has too much mixing regardless of cloudiness (Graham, Cohen, et al. 2019; Chang et al. 2021). An interesting aspect in OBS (but not ERA5) LWC profiles is that the calmer the conditions, the lower the altitude of the cloud liquid layer is situated. This shows that large-scale synoptic conditions impact the vertical distribution of mixed-phase clouds and hence the altitude of the most strongly emitting layers; they are shallow in the more stratified atmosphere during calm conditions and more elevated in deeper cloud systems present during strong synoptic forcing with deeper ABLs. Figure S4 supports this result by showing that the altitude of maximum LWC tends to peak in the lowermost 1000 m, especially for ERA5, where it rarely exceeds 2000 m. In OBS, however, the altitude of maximum LWC often exceeds 2000 m, especially for W2C2 and W1C2. ERA5 further underestimates IWC by approximately an order of magnitude for all classes, which is beyond the observational uncertainty.

Figure 4 emphasizes the differences between OBS and ERA5 temperature profiles from Figure 3. Here, synoptic classes are put in context with the classical radiatively opaque and radiatively clear state (as determined from LWnet, Stramler et al. 2011). For the

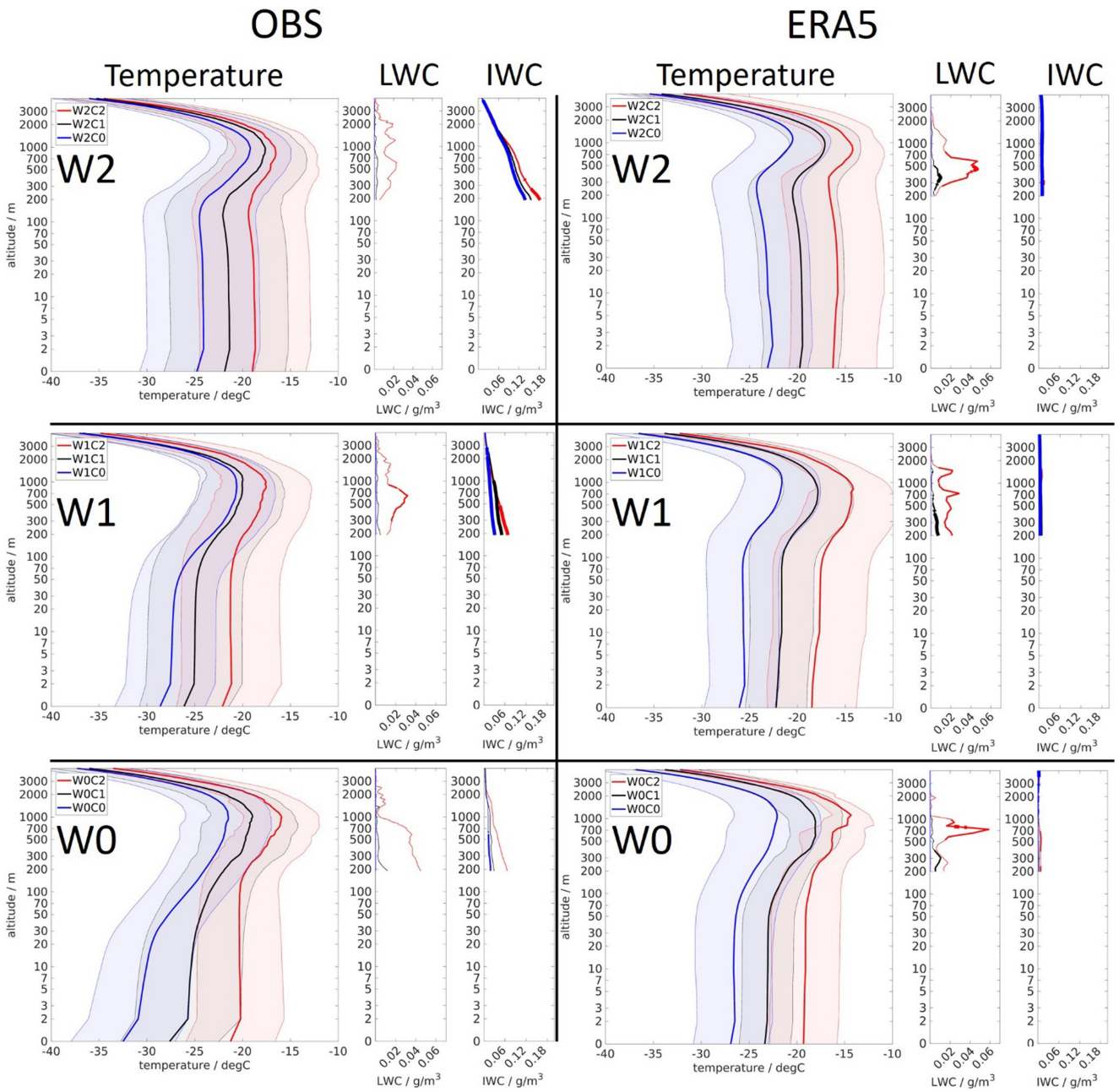

FIGURE 3 | Each panel shows average vertical profiles of temperature (large left inset per panel), LWC (small inset in the middle of each panel) and IWC (small inset in the right of each panel). Note that due to observational limitations of the radar, LWC and IWC are omitted below 200 m. Different colors indicate different synoptic classes, from W2 (top) to W1 (middle) to W0 (bottom) classes. Panels on the left are for OBS, and panels on the right are for ERA5. Shading around the temperature profiles indicates ±1 standard deviation. A bold (very bold) line in LWC and IWC profiles indicates that in at least 25 (50) percent of the cases in the class, LWC/IWC values exceeding 0.1 gm^{-3} are present at that height. Note the logarithmic *y*-axis for highlighting the near-surface and ABL region.

radiatively clear state, ERA5's warm bias has a pronounced vertical structure with strongest warm anomalies (+4.2 K) close to the surface and decreasing upwards until the bias becomes negligible at around 150 m altitude. This reflects the lack of SBIs in ERA5 and its surface warm bias. During the radiatively opaque state, the warm bias is weaker (+2 K), and uniform with altitude to 200 m height where it diminishes. Those biases are reflected in the combined wind-cloud classes as follows: At and close to the surface, ERA5 consistently shows a warm bias up to at least 100 m. For all C0 classes this warm bias diminishes upwards and turns to a cold bias above 100–200 m height. Judging from Figure 3, this may reflect that ERA5 misrepresents the altitudes of low-level ice clouds and corresponding cloud-top inversions, or an overestimation of the ABL height, as shown for MOSAiC by Xi et al. (2024). In W2 classes, compared to W1-W0 classes, the ERA5 surface warm bias is smallest (1.8–2.6 K), however, it is strongest (2.6 K) for W2C2, and weakest (1.8 K) for W2C0. This indicates that not only for calm and clear conditions, but also for strong synoptic forcing, the thermodynamic structure in ERA5 is biased, especially when extensive mixed-phase clouds are involved (Engström et al. 2014). In contrast, during W0, compared to W2–W1 classes, the near-surface temperature bias of ERA5 is generally largest,

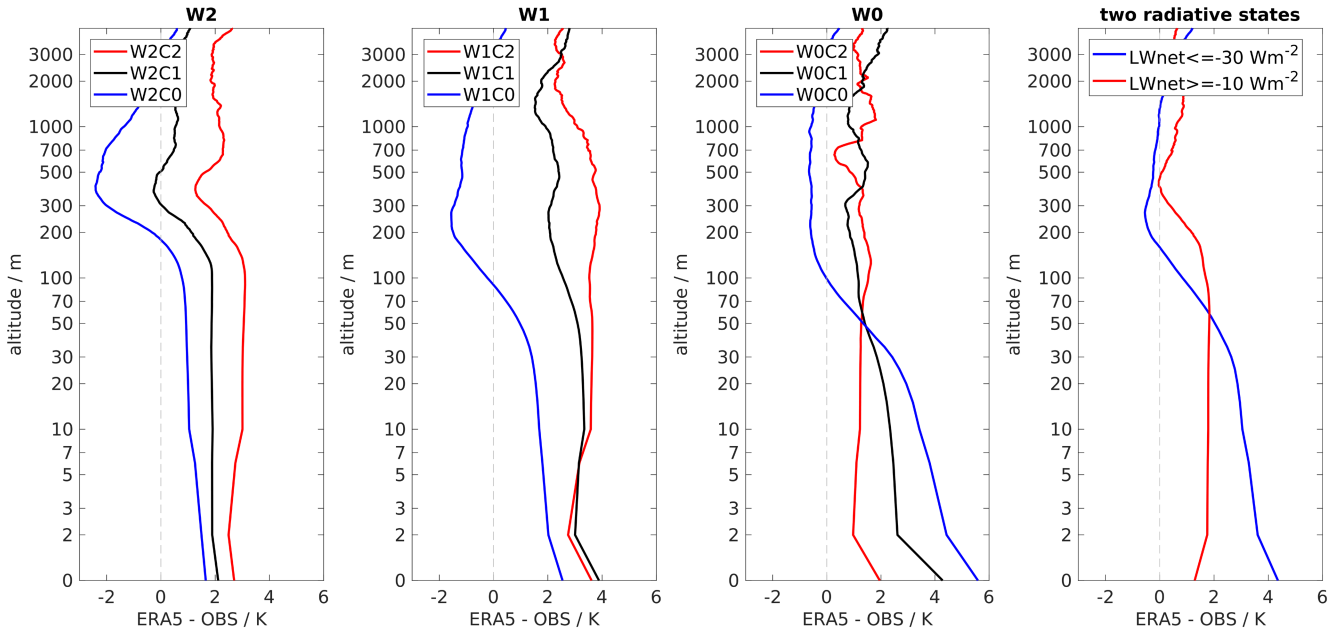

FIGURE 4 | ERA5 minus OBS differences in the average temperature profiles for each synoptic class that are shown in Figure 3. From left to right, the W2, W1, and W0 classes are shown. The right panel shows the average profiles for the classical radiative states, as defined by LWnet $\leq -30\,\mathrm{Wm}^{-2}$ (radiatively clear state) and LWnet $\geq -10\,\mathrm{Wm}^{-2}$ (radiatively cloudy/opaque state).

and shows a pronounced inversion structure, especially for W0C0 (5.8 K) rather than for W0C2 (< 2 K). Interestingly, the C0 class is the one with the largest warm bias during W0 conditions but is also the one with the smallest bias for W1 and W2 sub-classes. This emphasizes the problematic representation of shallow, stable ABLs during calm and clear conditions. Specifically, the ERA5-OBS discrepancy for the radiatively clear state (Figure 4) strongly resembles the W0C0 bias profile, with near surface biases exceeding 4 K, which is not present for any other class than W0C0. The W1 classes are the transition between the W2 and the W0 classes in terms of the vertical structure of the temperature bias.

Notably, the main biases depicted in Figure 4 also persist for ERA5-OBS events that are collocated in time (not shown), although radiosondes are assimilated in ERA5, which points to processes rather than temporal sampling differences as drivers of the biases.

3 | Discussion and Conclusion

ERA5 does not accurately simulate the bimodal states of the Arctic atmosphere, which is the primary synoptic-scale driver of variability in the energy balance over sea ice. Because ERA5 uses a dynamical model, the distinction between synoptic states should, to first order, be expected to be accurately simulated. While most studies treat the problem in the aggregate of conditions (e.g., Solomon et al. 2023) or continuously (e.g., Day et al. 2024), here we disaggregate and conduct an evaluation using synoptic classes. We focus on long-standing model biases for the Arctic winter climate, such as the surface warm bias with weak stratification, cloud water/ice partitioning, or the lack of bimodality in the LWnet distribution (Stramler et al. 2011; Pithan et al. 2014; Solomon et al. 2023). The distributions of the individual classes representing synoptic activity are qualitatively present in subsets of the overall distributions, but these classes are biased such that they overlap more in the aggregate distribution than observed.

Consistent with ERA5, enhanced LWP, especially under windy rather than calm conditions, contributes to the radiatively opaque state, while the radiatively clear state occurs in the absence of cloud liquid. Distinctive occurrence peaks of the W0 and W1 classes form the radiatively clear state in LWdown and LWnet, which are not captured in ERA5. The radiatively opaque state can also occur in the absence of liquid-bearing clouds, especially under strong winds. During such events, lower tropospheric ice clouds, water vapor, and warm air masses can also impact emissivity and LWdown. It is intriguing that ERA5 overestimates LWdown for all C0 classes, which can neither be explained by biases in LWP, IWP, or water vapor (Männel et al. 2021), nor by warm anomalies above 100 m height. This result rather suggests that the emitting layer tends to be lower, i.e., within the lowest 100 m, where warm biases persist. This finding is consistent with Ohmura (2001), who shows that in a cloud-free atmosphere, about 70% of LWdown originates from the lowermost 100 m.

Thermodynamic profiles reveal that ERA5's warm bias close to the surface is evident for all classes, but strongest during calm-, and weakest during windy conditions. For W0C0, the warm bias is shallow (~70 m) and with a pronounced inversion structure, while it reaches higher (~200 m) and is more isothermal for W2C0. This shows that ABL stability, vertical mixing, and the synoptic forcing altogether influence the performance of the reanalysis regarding the thermodynamic structure—a possible focus for dedicated future process studies. For example, downward mixing of sensible heat due to a warm-biased atmosphere may also contribute to ERA5's surface warm bias, but this is beyond the scope of this study. Moreover, frontal evolution of

cyclones produces variable forcing (Persson et al. 2017) and consequently, reanalysis models such as ERA5 can have varying biases within individual synoptic events, which are not distinguishable in the present analysis. Leads can impact the ABL locally, but we do not believe that this affected the aggregate of observations, because leads occurred generally downwind of the observations, and refroze quickly in the cold season (Sledd et al. 2025). Observations from the central Arctic are limited, especially for winter which shows the strongest changes (Rantanen et al. 2022). Future campaigns are needed alongside dedicated modeling to assess process representation and -relationships of the coupled Arctic climate system. The class-based approach described here is a promising tool for isolating physical processes responsible for errors.

Author Contributions

S.D. and A.R. conceptualized the study. S.D. and A.R. wrote the manuscript. S.D., C.J.C., and M.D.S. contributed meteorological data. All authors commented and edited the manuscript.

Acknowledgements

Data used in this manuscript were produced as part of the international Multidisciplinary drifting Observatory for the Study of Arctic Climate (MOSAiC) with the tag MOSAiC20192020. We thank all persons involved in the expedition of the Research Vessel Polarstern during MOSAiC in 2019–2020 (AWI_PS122_00) as listed in Nixdorf et al. (2021). Radiation and cloud information was obtained from the Atmospheric Radiation Measurement (ARM) User Facility, a U.S. Department of Energy (DOE) Office of Science User Facility managed by the Biological and Environmental Research Program. Radiosonde data were obtained through a partnership between the leading Alfred Wegener Institute (AWI), the DOE ARM facility, and the German Weather Service (DWD). Meteorological data was obtained from the University of Colorado/NOAA surface flux team. Open Access funding enabled and organized by Projekt DEAL.

Conflicts of Interest

The authors declare no conflicts of interest.

Data Availability Statement

The observational data that support the findings of this study are openly available in PANGAEA at https://doi.pangaea.de/10.1594/PANGAEA.961881, as well as in the Arctic Data Center at https://arcticdata.io/catalog/view/doi:10.18739/A2PV6B83F, and in the ARM data repository at https://doi.org/10.5439/1871015. ERA5 reanalysis data are publicly accessible via the Climate Data Store (CDS).

References

Arduini, G., S. Keeley, J. J. Day, I. Sandu, L. Zampieri, and G. Balsamo. 2022. "On the Importance of Representing Snow Over Sea-Ice for Simulating the Arctic Boundary Layer." *Journal of Advances in Modeling Earth Systems* 14: e2021MS002777. https://doi.org/10.1029/2021MS002777.

Batrak, Y., and M. Müller. 2019. "On the Warm Bias in Atmospheric Reanalyses Induced By the Missing Snow Over Arctic Sea-Ice." *Nature Communications* 10: 4170. https://doi.org/10.1038/s41467-019-11975-3.

Chang, L., S. Wen, G. Gao, Z. Han, G. Feng, and Y. Zhang. 2021. "Assessment of Temperature and Specific Humidity Inversions and Their Relationships in Three Global Reanalysis Products Over the Arctic Ocean." *Journal of Applied Meteorology and Climatology* 60, no. 4: 493–511. https://doi.org/10.1175/jamc-d-20-0079.1.

Cox, C. J., M. R. Gallagher, M. D. Shupe, et al. 2023. "Continuous Observations of the Surface Energy Budget and Meteorology Over the Arctic Sea Ice During Mosaic." *Scientific Data* 10: 519. https://doi.org/10.1038/s41597-023-02415-5.

Dahlke, S., M. D. Shupe, C. J. Cox, I. M. Brooks, B. Blomquist, and P. O. G. Persson. 2023. "Extended Radiosonde Profiles 2019/09-2020/10 During MOSAiC Legs PS122/1–PS122/5 [Dataset]. PANGAEA." https://doi.org/10.1594/PANGAEA.961881.

Day, J. J., G. Svensson, B. Casati, et al. 2024. "The Year of Polar Prediction Site Model Intercomparison Project (Yoppsitemip) Phase 1: Project Overview And Arctic Winter Forecast Evaluation." *Geoscientific Model Development* 17: 5511–5543. https://doi.org/10.5194/gmd-17-5511-2024.

Engström, A., J. Karlsson, and G. Svensson. 2014. "The Importance of Representing Mixed-Phase Clouds For Simulating Distinctive Atmospheric States in the Arctic." *Journal of Climate* 27, no. 1: 265–272. https://doi.org/10.1175/JCLI-D-13-00271.1.

Graham, R. M., A. Rinke, L. Cohen, et al. 2017. "A Comparison of the Two Arctic Atmospheric Winter States Observed During N-Ice2015 And Sheba." *Journal of Geophysical Research-Atmospheres* 122: 5716–5737. https://doi.org/10.1002/2016JD025475.

Graham, R. M., S. R. Hudson, and M. Maturilli. 2019. "Improved Performance of ERA5 in Arctic Gateway Relative to Four Global Atmospheric Reanalyses." *Geophysical Research Letters* 46: 6138–6147. https://doi.org/10.1029/2019GL082781.

Graham, R. M., L. Cohen, N. Ritzhaupt, et al. 2019. "Evaluation of Six Atmospheric Reanalyses Over Arctic Sea Ice From Winter to Early Summer." *Journal of Climate* 32: 4121–4143. https://doi.org/10.1175/JCLI-D-18-0643.1.

Herrmannsdörfer, L., M. Müller, M. D. Shupe, and P. Rostosky. 2023. "Surface Temperature Comparison of the Arctic Winter MOSAiC Observations, ERA5 Reanalysis, and MODIS Satellite Retrieval." *Elementa: Science of the Anthropocene* 11, no. 1: 00085. https://doi.org/10.1525/elementa.2022.00085.

Hersbach, H., B. Bell, P. Berrisford, et al. 2020. "The ERA5 Global Reanalysis." *Quarterly Journal of the Royal Meteorological Society* 146: 1999–2049. https://doi.org/10.1002/qj.3803.

Männel, B., F. Zus, G. Dick, et al. 2021. "GNSS-Based Water Vapor Estimation and Validation During the MOSAiC Expedition." *Atmospheric Measurement Techniques* 14: 5127–5138. https://doi.org/10.5194/amt-14-5127-2021.

Miller, N., M. Shupe, C. Cox, V. Walden, D. Turner, and K. Steffen. 2015. "Cloud Radiative Forcing at Summit, Greenland." *Journal of Climate* 28, no. 15: 6267–6280. https://doi.org/10.1175/JCLI-D-15-0076.1.

Morrison, H., G. de Boer, G. Feingold, J. Harrington, M. D. Shupe, and K. Sulia. 2012. "Resilience of Persistent Arctic Mixed-Phase Clouds." *Nature Geoscience* 5: 11–17. https://doi.org/10.1038/ngeo1332.

Nixdorf, U., K. Dethloff, M. Rex, et al. 2021. "MOSAiC Extended Acknowledgement. Zenodo." https://doi.org/10.5281/zenodo.5541624.

Ohmura, A. 2001. "Physical Basis For the Temperature-Based Melt-Index Method." *Journal of Applied Meteorology and Climatology* 40, no. 4: 753–761. https://doi.org/10.1175/1520-0450(2001)040<0753:PBFTTB>2.0.CO;2.

Pithan, F., B. Medeiros, and T. Mauritsen. 2014. "Mixed-Phase Clouds Cause Climate Model Biases in Arctic Wintertime Temperature Inversions." *Climate Dynamics* 43: 289–303. https://doi.org/10.1007/s00382-013-1964-9.

Persson, P. O. G., M. D. Shupe, D. Perovich, and A. Solomon. 2017. "Linking Atmospheric Synoptic Transport, Cloud Phase, Surface Energy Fluxes, and Sea-Ice Growth: Observations of Midwinter SHEBA

Conditions." *Climate Dynamics* 49: 1341–1364. https://doi.org/10.1007/s00382-016-3383-1.

Rantanen, M., A. Y. Karpechko, A. Lipponen, et al. 2022. "The Arctic has Warmed Nearly Four Times Faster Than the Globe Since 1979." *Communications Earth and Environment* 3: 168. https://doi.org/10.1038/s43247-022-00498-3.

Shupe, M. D., and J. M. Intrieri. 2004. "Cloud Radiative Forcing of the Arctic Surface: The Influence of Cloud Properties, Surface Albedo, and Solar Zenith Angle." *Journal of Climate* 17: 616–628. https://doi.org/10.1175/1520-0442(2004)017<0616:CRFOTA>2.0.CO;2.

Shupe, M. D., T. Uttal, and S. Matrosov. 2005. "Arctic Cloud Microphysics Retrievals From Surface-Based Remote Sensors at SHEBA." *Journal of Applied Meteorology and Climatology* 44, no. 10: 1544–1562. https://doi.org/10.1175/JAM2297.1.

Shupe, M. D., D. D. Turner, A. Zwink, M. M. Thieman, E. J. Mlawer, and T. Shippert. 2015. "Deriving Arctic Cloud Microphysics at Barrow, Alaska: Algorithms, Results, and Radiative Closure." *Journal of Applied Meteorology and Climatology* 54: 1675–1689. https://doi.org/10.1175/JAMC-D-15-0054.1.

Shupe, M. D. 2022. "ShupeTurner Cloud Microphysics." https://doi.org/10.5439/1871015.

Shupe, M., M. D. Shupe, M. Rex, et al. 2022. "Overview of the MOSAiC Expedition: Atmosphere." *Elementa: Science of the Anthropocene* 10, no. 1: 00060. https://doi.org/10.1525/elementa.2021.00060.

Sledd, A., M. D. Shupe, A. Solomon, and C. J. Cox. 2025. "Surface Energy Balance Responses to Radiative Forcing in the Central Arctic from MOSAiC and Models." *Journal of Geophysical Research: Atmospheres* 130: e2024JD042578. https://doi.org/10.1029/2024JD042578.

Solomon, A., M. D. Shupe, G. Svensson, et al. 2023. "The Winter Central Arctic Surface Energy Budget: A Model Evaluation Using Observations From the MOSAiC Campaign." *Elementa: Science of the Anthropocene* 11, no. 1: 00104. https://doi.org/10.1525/elementa.2022.00104.

Stramler, K., A. D. Del Genio, and W. B. Rossow. 2011. "Synoptically Driven Arctic Winter States." *Journal of Climate* 24: 1747–1762. https://doi.org/10.1175/2010JCLI3817.1.

Svensson, G., S. Murto, M. D. Shupe, et al. 2023. "Warm Air Intrusions Reaching the MOSAiC Expedition in April 2020—TheYOPP Targeted Observing Period (TOP)." *Elementa: Science of the Anthropocene* 11, no. 1: 00016. https://doi.org/10.1525/elementa.2023.00016.

Tjernström, M., and R. G. Graversen. 2009. "The Vertical Structure of the Lower Arctic Troposphere Analysed From Observations and the ERA-40 Reanalysis." *Quarterly Journal of the Royal Meteorological Society* 135: 431–443. https://doi.org/10.1002/qj.380.

Vihma, T., and R. Pirazzini. 2005. "On the Factors Controlling the Snow Surface and 2-m Air Temperatures Over the Arctic Sea Ice in Winter." *Boundary-Layer Meteorology* 117: 73–90. https://doi.org/10.1007/s10546-004-5938-7.

Walsh, J. E., and W. L. Chapman. 1998. "Arctic Cloud-Radiation-Temperature Associations in Observational Data and Atmospheric Reanalyses." *Journal of Climate* 11: 3030–3045.

Xi, X., Q. Yang, C. Liu, et al. 2024. "Evaluation of the Planetary Boundary Layer Height From ERA5 Reanalysis With MOSAiC Observations Over the Arctic Ocean." *Journal of Geophysical Research: Atmospheres* 129: e2024JD040779. https://doi.org/10.1029/2024JD040779.

Supporting Information

Additional supporting information can be found online in the Supporting Information section.